Identifying Debonding Regions in a Composite Radiative Cooling Film Bonded to a Steel Plate

P. SHIVASHANKAR, ANGELA WHITTLE
and SALVATORE SALAMONE

ABSTRACT

This study presents a method to map the regions of debonding of a thin composite film attached to a steel plate based on the changes in Lamb wave signatures. The film in discussion is a passive radiative cooling film that can be coated on the top of metallic roof shingles to reflect the sunlight and subsequently cool the building. It is an energy-efficient building material that can potentially reduce building energy consumption by up to 30%. Its effectiveness can, however, be decreased by damage or debonding of the film from the substructure. Hence, it is essential to identify the regions of debonding/damage in a timely manner for rectification. Here, we demonstrate a method to map the regions of debonding based on changes observed in Lamb waves when they pass through a debonded region. When the Lamb waves pass through this film, they get attenuated and arrive with a slight delay. By quantifying the changes in the wavepackets, the debonded regions can be mapped tomographically. With this as the basis, experiments were conducted on a steel plate bonded with the film to demonstrate the mapping of debonded regions. A small section of the film was removed to simulate a damaged scenario. PZT discs were bonded to the structure along the edges of the square to create a dense network of paths passing through the film. Along each path, signals are acquired in pristine and damaged conditions to estimate the damage index for each path. The Reconstruction Algorithm for Probabilistic Inspection of Damage (RAPID) technique was employed to construct the map, where high-intensity regions denoted areas with a higher likelihood of debonding. The obtained map was compared with the structure to validate the method and establish it as a viable option. Through a successful demonstration, this work lays the foundations for identifying and quantifying regions of film debonding.

INTRODUCTION

Structures like buildings require access to electricity, and in the United States of America, this accounts for over 40% of total energy consumption. Given this, there has been an increased interest in innovations for reducing buildings' energy consump-

P Shivashankar, A Whittle, & S Salamone, Smart Structures Research Laboratory, Maseeh Department of Civil, Architectural and Environmental Engineering, The University of Texas at Austin, Austin, TX 78712, USA

tion [1]. One option for reducing energy consumption is a composite passive radiative cooling (CRC) film [2], which utilizes radiative cooling technology to maintain a cool environment within buildings. This, in turn, reduces the energy consumption of buildings and other housing structures, such as hangars and tents. The successful implementation of these types of film can result in a decrease of up to 30% in energy usage [3].

However, due to various factors, the film may debond from the structure, leading to a decrease in cooling effectiveness. Hence, it is essential that these regions of debonding be identified and rectified for an effective operation. Accordingly, this study presents a comprehensive methodology for identifying such defective areas and monitoring their growth over time.

The mapping of debonded regions is based on the change in the Lamb wave signature when it propagates through a debonded region. Lamb waves, a category of dispersive ultrasonic waves that propagate in thin plate-like structures, are a valuable tool for non-destructive evaluation (NDE) due to their ability to travel long distances with minimal energy loss. When these waves propagate through the film, they get attenuated and arrive with a slight delay–a behavior very similar to that observed in protective coatings on metallic structures [4, 5]. By quantifying the changes in the propagating waves, the regions of debonding can be mapped using tomographic methods, such as RAPID.

This study demonstrates the methodology for mapping debonded regions on a steel plate covered with the CRC film. The following section outlines the test specimen and the experimental setup used in the study. The section after that describes the imaging algorithm and presents the results. The final section concludes the paper by discussing the key findings and the scope for future research.

EXPERIMENT

The test structure used in the experiments consists of a steel plate bonded with CRC film. The plate is of dimensions 48"$\times$ 48"$\times$ 0.036", while the film's thickness is estimated to be in the range of 0.05–0.1 mm. This steel plate was propped up with eight foam blocks, which were placed along the edges of the plate. Figure 1a shows the plate being placed on the foam supports. The center region of the plate was chosen as the test site, where twenty PZT discs were evenly distributed along the edges of a 33 cm $\times$ 33 cm square. Figure 1b shows the PZT discs bonded to the plate. The target area was a 30.5 cm $\times$ 30 cm region within the PZT square, where the film is bonded. The PZT discs had a diameter of 6.35 mm and a thickness of 0.635 mm. They were of Type 850 from APC International Ltd. They were bonded to the structure with the two-part Araldite epoxy.

One at a time, each PZT transducer was used as an actuator to generate Lamb waves. When one transducer was used as an actuator, the remaining PZTs, not on the same edge, were used as sensors. Figure 2a illustrates the paths for one scenario, where PZT-1 is used as the actuator and PZTs 6-20 are used as sensors. All combinations of actuators and sensors result in a dense network of paths that pass through the target area. Figure 2b shows the network of paths formed by the transducers.

For the purposes of testing, an artificial debonding scenario was achieved by removing a small section of the film. Specifically, a 4 cm $\times$ 4 cm section was entirely

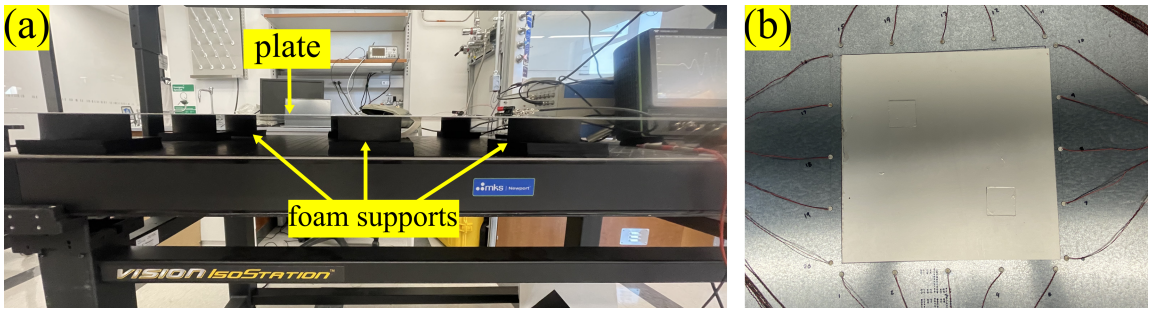

Figure 1. (a) The plate placed on foam supports, and (b) PZT discs distributed in the perimeter of a square around the bonded film.

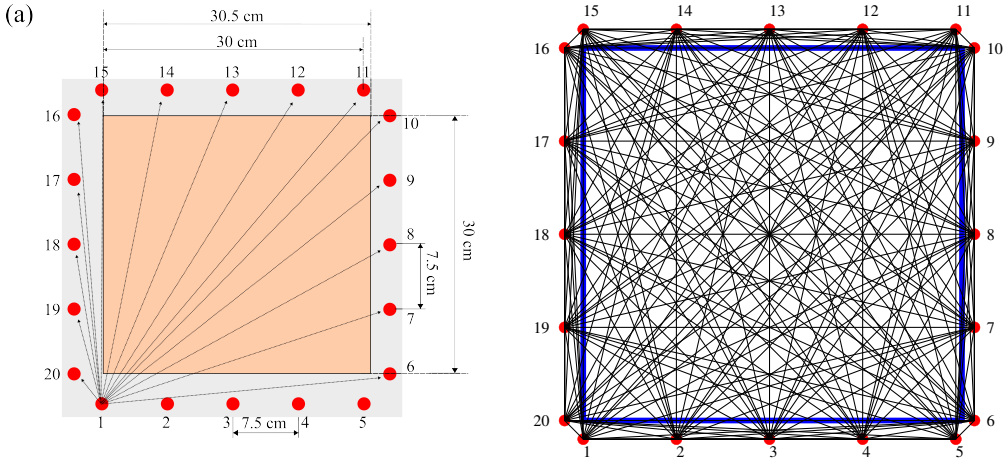

Figure 2. (a) The paths from A1 to S6-S20, and (b) the network of paths from all combinations of transducers.

removed to mimic a debonded region. Although this does not accurately replicate a real-life debonded condition, it still emulates the effect of debonding. While in practical situations, the film may still be physically present, the effect of a debonded segment and a missing segment may be functionally similar–namely, the absence of any connection between the film and the substrate. The "debonded" region was located near the top-left corner of the film, with its left and top edges positioned 7 cm away from the respective left and top edges of the film. Figure 3 shows and illustrates the "*damaged*" case.

The excitation signal was a 5-cycle tone burst with a center frequency of 150 kHz. The signal was generated by an Agilent 33522A waveform generator and amplified by a Ritec RPR4000 Pulser Receiver, which was set in the external mode. The propagating wave signals were acquired with an NI PXIe-5105 oscilloscope, which was housed in an NI PXIe-1071 chassis. At 150 kHz, S_0 and A_0 modes exist with respective wavelengths of 26 mm and 6.2 mm. Figure 4 shows the pristine and damaged signals for actuation from PZT disc No. 1 (Actuator-1) and the responses from PZT discs No. 8 (Sensor-8) and No. 13 (Sensor-13). The path A1-S8 does not go through the damage, but A1-S13 does. Consequently, the change in the signal is significant for the latter path. As such, the damage indexes estimated from the A_0 window for the respective paths are: $\mathcal{D}_{A1-S8} = 3.82 \times 10^{-4}$ and $\mathcal{D}_{A1-S13} = 1.79 \times 10^{-2}$. The damage indexes are evaluated

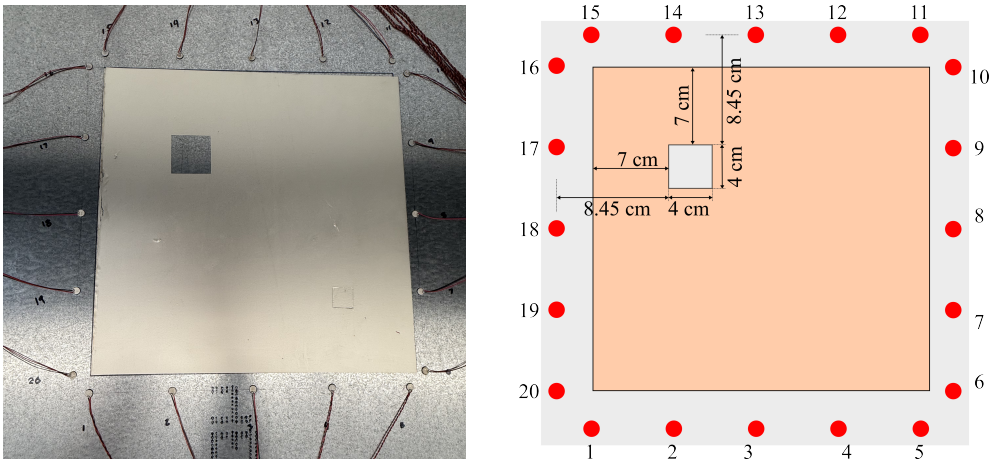

Figure 3. The damaged case and its schematic diagram.

from the following expression,

$$\mathcal{D} = \frac{\int_{t_1}^{t_2} \left[s_d(t) - s_p(t)\right]^2 dt}{\int_{t_1}^{t_2} \left[s_p(t)\right]^2 dt} \tag{1}$$

where, s_p and s_d indicate the pristine and damaged signals, respectively, and t_1 and t_2, the start and end times of the A_0 window.

With the damage indexes along all the paths, a map indicating the location of the damage is generated. The algorithm used to construct the map and the resulting tomographic image are presented in the following section.

TOMOGRAPHIC MAPPING THROUGH RAPID

RAPID

RAPID (Reconstruction Algorithm for Probabilistic Inspection of Damage) is an imaging technique used in structural health monitoring to identify and locate damage in a specified area. This technique utilizes predefined sensor locations within a probabilistic framework to reconstruct images that show the location of damage. Specifically, the map is constructed by aggregating damage information from each individual path. That is, the constructed map is made by summing together the defect distributions of all transducer pairs. The defect distribution for any transducer pair, say the k^{th} pair, is estimated according to,

$$p_k\left(x, y\right) = \mathcal{D}_k\left(\frac{-R_k\left(x, y\right)}{\beta - 1} + \frac{\beta}{\beta - 1}\right) \tag{2}$$

where

$$R_k\left(x, y\right) = \frac{\sqrt{\left(x - x_k^{(A)}\right)^2 + \left(y - y_k^{(A)}\right)^2} + \sqrt{\left(x - x_k^{(S)}\right)^2 + \left(y - y_k^{(S)}\right)^2}}{\sqrt{\left(x_k^{(S)} - x_k^{(A)}\right)^2 + \left(y_k^{(S)} - y_k^{(A)}\right)^2}} \tag{3}$$

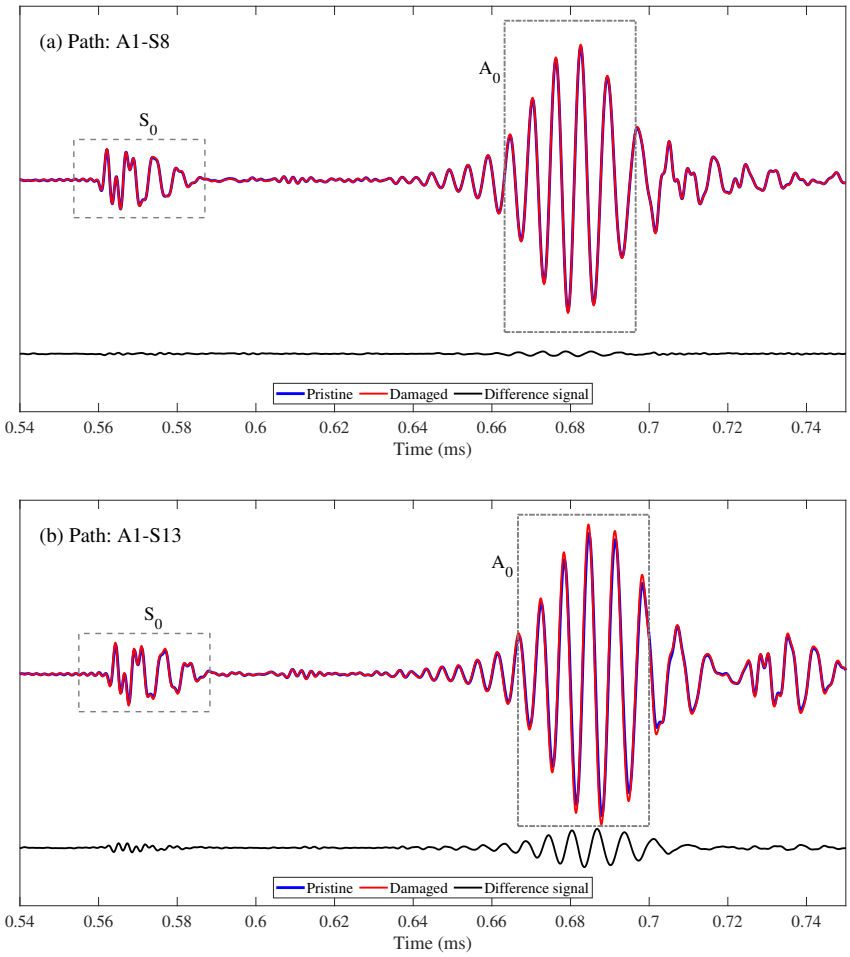

Figure 4. Pristine and damaged wave responses, along with the difference signal, along the paths connecting (a) PZT-1 (actuator-1) and PZT-8 (sensor-8), and (b) PZT-1 (actuator-1) and PZT-13 (sensor-13).

(x, y) denote the coordinates of any point on map, and $\left(x_k^{(A)}, y_k^{(A)}\right)$ and $\left(x_k^{(S)}, y_k^{(S)}\right)$ indicate the coordinates of the k^{th} transducer pair's actuator and sensor locations, respectively. β in Equation 2 is a scaling parameter.

Equation 2 generates a heat map with a set of concentric ellipses with the k^{th} transducer-pair coordinates at the foci. This heat map represents the spatial distribution of damage in the sub-area surrounding the k^{th} transducer pair. As such, the direct path connecting the transducers is specified to have the highest probability of containing the damage. Beyond this direct path, this probability progressively diminishes with each successive elliptical contour. The final heat map–which indicates the presence of the damage–is a sum of the spatial damage distributions of all transducer pairs. As such, the contour map of the structure is generated from the following equation.

$$P(x, y) = \sum_{k=1}^{k=N} p_k(x, y) \tag{4}$$

TOMOGRAPHIC IMAGE

Figure 5 shows the heat map generated through RAPID with information from the 150

transducer pairs. A region of higher intensity implies a larger damage index zone and, in turn, the presence of damage. Cross-referencing the heat map with Figure 3 shows that the high-intensity region is in the same locality as the damage. To identify the exact location of the damage, a pixel intensity threshold of 0.85 was chosen, and regions with intensities higher than this threshold were designated as containing the damage. Regions with pixel intensities above 0.85 were demarcated and marked as potential regions containing the damage. The contour in the image marks the high-intensity region. The second image superimposes this region on the schematic diagram, wherein it can be seen that the region identified from the experiments closely matches the actual damaged area (i.e., the debonded region).

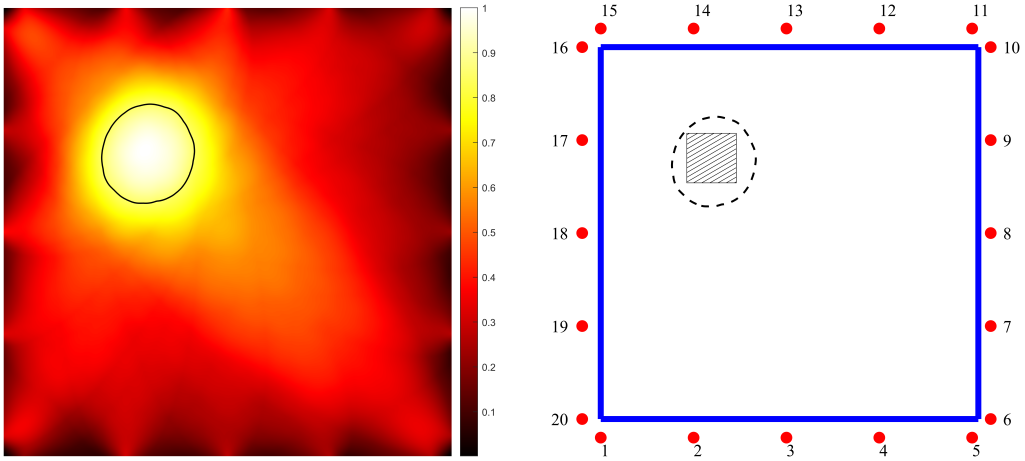

Figure 5. The tomographic image obtained from RAPID, with the contour denoting the region of high intensity, and the figure superimposing the high-intensity contour region on the schematic diagram.

The threshold dictates the size of the estimated defect. A larger threshold would shrink the estimated region, with an area value closer to the actual one. Another alternative to obtain a more accurate estimate would be to use Lamb waves with shorter wavelengths. This will be investigated in future studies.

The successful detection of the debonding region establishes the Lamb-based tomographic mapping as a valid option for locating damages in the bonded film. With this study as a starting point, future research will explore different excitation frequencies, defect sizes, and the presence of multiple defects and provide a comprehensive guideline for real-world implementation.

CONCLUSION

This work investigated the possibility of using guided ultrasonic waves to locate regions of debonding of a composite passive radiative cooling (CRC) film. A thin steel plate with the CRC film bonded to its surface was chosen as the test specimen. A small section of the film was removed to simulate a debonding damage. PZT discs were bonded around the perimeter of the test region to generate and receive the Lamb waves. The evenly distributed transducer array created a dense network of paths that passed

through the test area. When the wave passes through a film-bonded region, it gets attenuated and delayed. This change in the signature of the wave packet serves as an indication of the presence (or absence) of the film. The A_0 mode was excited, and based on the changes to the wave packet caused by "debonding," the debonded regions were successfully mapped using the RAPID method. The successful demonstration showcases the method's capability in identifying areas of film damage. With this as a starting point, future studies will investigate the presence of multiple damages of varying sizes and subsequently extend the method for real-world implementation.

ACKNOWLEDGMENT

The authors thank the Air Force Research Laboratory for supporting this work through the Contract No. FA8650-21-C-5018. We also extend our thanks to PC Krause & Associates and Prof. Atila Novoselac of UT Austin for providing the film and the plate for testing. Their support and guidance was invaluable for undertaking this study.

REFERENCES

1. NREL. 2023, "NREL Researchers Reveal How Buildings Across the United States Do and Could Use Energy," https://www.nrel.gov/news/detail/features/2023/nrel-researchers-reveal-how-buildings-across-the-united-states-do-and-could-use-energy, accessed: 2024-11-10.
2. Heltzel, A. 2022, "Composite material for passive radiative cooling," US Patent 11,440,291.
3. Zhao, D., A. Aili, Y. Zhai, S. Xu, G. Tan, X. Yin, and R. Yang. 2019. "Radiative sky cooling: Fundamental principles, materials, and applications," *Applied Physics Reviews*, 6(2).
4. Barshinger, J. N. and J. L. Rose. 2004. "Guided wave propagation in an elastic hollow cylinder coated with a viscoelastic material," *IEEE transactions on ultrasonics, ferroelectrics, and frequency control*, 51(11):1547–1556.
5. Van Velsor, J. K. 2009. *Circumferential guided waves in elastic and viscoelastic multilayered annuli*, The Pennsylvania State University.